*Desalination and Water Treatment*
www.deswater.com

doi: 10.5004/dwt.2020.24809

173 (2020) 394–408
January

# Ultra-fast removal of cadmium and lead from wastewater using high-efficient adsorbent derived from plastic waste: statistical modeling, kinetic and isotherm studies

Noha A. Elessawy[a], Marwa H. Gouda[b], Marwa F. Elkady[c], Safaa M. Ali[d], M. Gouda[e,*], Mohamed S. Mohy Eldin[b,*]

[a]*Advanced Technology and New Materials Research Institute, City of Scientific Research and Technological Applications (SRTA-City), New Borg El-Arab City, 21934 Alexandria, Egypt, email: nony_essawy@yahoo.com*
[b]*Polymer Materials Research Department, Advanced Technology and New Materials Research Institute, City of Scientific Research and Technological Applications (SRTA-City), New Borg El-Arab City, 21934 Alexandria, Egypt, emails: mmohyeldin@srtacity.sci.eg (M.S.M. Eldin), marwagouda17@yahoo.com (M.H. Gouda)*
[c]*Chemical and Petrochemical Engineering Department, Egypt-Japan University of Science and Technology (E-JUST), New Borg El-Arab City, 21934 Alexandria, Egypt, email: marwa.f.elkady@gmail.com*
[d]*Nucleic Acid Research Department, Genetic Engineering and Biotechnology Research Institute (GEBRI), City of Scientific Research and Technological Applications (SRTA-City), New Borg El-Arab City, 21934 Alexandria, Egypt, email: Safaa.mohamedali@yahoo.com*
[e]*Chemistry Department, College of Science, King Faisal University, Al-Hassa, Saudi Arabia, email: mgoudaam@kfu.edu.sa*

Received 9 April 2019; Accepted 23 August 2019

**ABSTRACT**

Magnetic sulfonated graphene (MSG) composite was synthesized from polyethylene terephthalate bottle waste by using a facile and reproducible method in addition to two graphene-based nanomaterials, including highly reduced graphene oxide (HRGO) and sulfonated graphene (SG). Further, batch experiments were carried out to examine their adsorption efficiency in relation to two heavy metals ions, Cd(II) and Pb(II), in single metal and mixed-metal solutions. The synthesized materials were characterized by Fourier transform infrared, X-ray diffraction, transmission electron microscope, energy dispersive X-Ray spectroscopy, and Brunauer–Emmett–Teller analysis which indicated that HRGO was successfully decorated by sulfonic groups and magnetic nanoparticles. Operating parameters including time, initial concentration of metal and adsorbent dose on the adsorption process were investigated and optimized at a pH of 5.5 for both metals using a response surface methodology model; however, the optimum conditions for Cd(II) removal were 13.28 min contact time, 50 mg $L^{-1}$ of Cd(II) initial concentration, and 0.012 mg of MSG at 25°C while, at contact time 2.9 min, 100.7 mg $L^{-1}$ of Pb(II) and 0.14 mg of MSG, complete removal was achieved. Adsorption process was obeyed pseudo-second-order and intra-particle diffusion kinetic models, while the calculated adsorption capacities of MSG for Cd(II) and Pb(II) ions at equilibrium fit perfectly with Langmuir and Freundlich isotherms models. The negative values of $\Delta G$ and positive values of $\Delta H$ and $\Delta S$ elucidate that the adsorption of Cd(II) and Pb(II) ions onto MSG is spontaneous, endothermic and random process. In addition, the adsorbents were easily regenerated and reused for five cycles with high adsorption capacity. This study indicates that the prepared MSG is a low-cost reusable adsorbent for the rapid and efficient removal of Cd(II) and Pb(II) ions from contaminated wastewater.

*Keywords:* Graphene-based adsorbent; Cd(II) and Pb(II) ions; Adsorption; Kinetics; Isotherm; Thermodynamics

* Corresponding authors.

## 1. Introduction

In the recent years, water sources on our planet got polluted by various toxic heavy metals further away than their permissible limits due to speedily growing industrialization and that in turn poses a potential risk to ecological balance and affects human health. Heavy metals ions as Cd(II) and Pb(II) are commonly found in the air, water as well as in the soil and they attracted a worldwide concern due to their high toxicity on the living beings whereas Cd can cause cell death, kidney, bone disease and lung function damage [1] while Pb can cause serious blood diseases [2], furthermore these elements are non-biodegradable [3]. The maximum permissible limits of heavy metals as cadmium and lead had been set for drinking water by World Health Organization at 0.003 mg $L^{-1}$ for Cd(II) and 0.01 mg $L^{-1}$ for Pb(II) because these metals can be easily accumulated inside living organisms and consequently endangering the public health. To solve this problem, many treatment techniques have been studied to eliminate heavy metals from wastewater, including ion exchange [4], coagulation [5], adsorption [6–8], membrane techniques [9] and bio-sorption [10]. Adsorption is a promising method because of its high efficiency, simple design and low-cost [11].

Graphene is a monolayer of carbon atoms packed into a honeycomb crystal plane with high surface area, superior electrical, thermal and mechanical properties which enabled it to be used in multidisciplinary field. However, the strong interaction between graphene sheets, which decrease the surface area and the absence of effective methods to disperse graphene in an aqueous solution significantly, reduces the development of graphene in pollutant removal [12]. Therefore, considerable efforts have been made to enhance graphene (G) water dispersibility. For instance, sulfonated graphene (SG) was synthesized as a good dispersibility graphene derivative in aqueous solutions and can be classified as a promising material for different applications because it has the π-π conjugated structure of graphene. The synthesis of graphene with sulfonic groups has been investigated in many studies, which essentially show that the routes significantly depend on three main points. The initial step consists of the synthesis of graphene oxide (GO) by graphite oxidative exfoliation using a modified Hummers method followed by adding sulfonating agents, such as chlorosulfonic acid [13,14], sulfuric acid [15,16], 4-diazoniobenzenesulfonate [17–19], and 2-chloroethanesulfonic acid [20], which have been used on graphene oxide and graphene. However, SG has been mostly used as an adsorbent for many pollutants, including 1-naphthol and naphthalene from aqueous solutions [21,22], dyes such as Malachite Green (MG) and Methylene Blue (MB) [23], and heavy metals ions [24,25]. Unfortunately, SG nanosheets pose difficulty in collection from wastewater after the adsorption process due to its nanosize and ease dispersion in water. Accordingly, the residual SG would cause secondary pollution in water. Therefore, the integration of magnetic particles on the surface of SG can realize the high adsorption capacity [26] of SG and easily separate the magnetic materials [12,24]; in addition, the metal pollutants can be attached to the magnetic materials through their outside active sites [27]. Generally, the adsorption ability of any material is controlled by the number of available functional groups. Therefore, inserting new functional groups onto graphene sheets leads to an increase in the adsorption capacity [24,28]. However, many studies have shown that material-based graphene can be used as an efficient adsorbent to remove heavy metals from wastewater [29] but it could not be used on practical scale due to its far high expensive nature than activated carbon (AC).

Herein, purify contaminated wastewater using waste materials, call the "wastes-treat-wastes" concept, is the aim of this study to achieve the benefits of both water treatment and waste management. Highly reduced graphene oxide (HRGO), sulfonated graphene (SG), and magnetic sulfonated graphene (MSG) were prepared using simple, one pot and applicable method as thermal dissociation of polyethylene terephthalate (PET) bottle waste [30] to produce cost-effective adsorbents. Subsequently, the effects of different adsorption process parameters on the removal of toxic metals as Cd(II) and Pb(II) in contaminated water onto prepared materials were explored and optimized. In addition, the adsorption kinetics, isotherms, thermodynamic and removal capacity were investigated for MSG through a series of adsorption experiments. Finally, the regeneration and recycling test parameters were also studied.

## 2. Materials and methods

### 2.1. Materials

Plastic bottles waste were taken as sources of PET and used to prepare HRGO and its derivatives multi nanosheets. Fuming sulfuric acid ($H_2SO_4$), ferric chloride hexahydrate ($FeCl_3{\cdot}6H_2O$), ferrous sulfate ($FeSO_4{\cdot}7H_2O$) and ammonium hydroxide ($NH_4OH$), $Cd(NO_3)_2{\cdot}4H_2O$ and $Pb(NO_3)_2$ were purchased from Sigma-Aldrich (USA). All solutions were prepared using deionized water.

### 2.2. Preparation of the functionalized graphene materials

The PET bottle waste was washed, dried and cut to be used as mentioned in a previous study [30]. Two grams of waste were introduced into an enclosed autoclave jar and placed inside the center of an electric furnace at 800°C for 1 h [31]. The resulting dark products were collected and crushed.

Sulfonated graphene (SG) nanosheets were prepared by the sulfonation of prepared HRGO using concentrated $H_2SO_4$ by adding 1 g of HRGO into 50 mL of concentrated $H_2SO_4$ [16,32] to introduce hydrophilic sulfonic acid groups ($SO_3H$) to the surface. The mixture was sonicated for 30 min and subsequently heated at 150°C under vigorous stirring for 24 h. Subsequently, the reaction mixture was cooled down to room temperature, then the mixture was filtered using vacuum pump, and washed with deionized water several times to remove any excess acid. The solid product was dried at 80°C for 12 h.

As shown in Fig. 1, MSG nanocomposite was synthesised based on the precursors of ferric chloride ($FeCl_3{\cdot}6H_2O$), ferrous sulfate ($FeSO_4{\cdot}7H_2O$), and the precipitator of ammonium hydroxide ($NH_4OH$) by using an inverse co-precipitation process [33]. 0.5 g of SG nanosheets were added to 20 mL of 0.2 M $NH_4OH$ aqueous solution into a 250 mL four-neck bottle and purged with $N_2$ atmosphere for 30 min. 1.08 g of $FeCl_3{\cdot}6H_2O$ and 0.54 g of $FeSO_4{\cdot}7H_2O$ with a stoichiometric

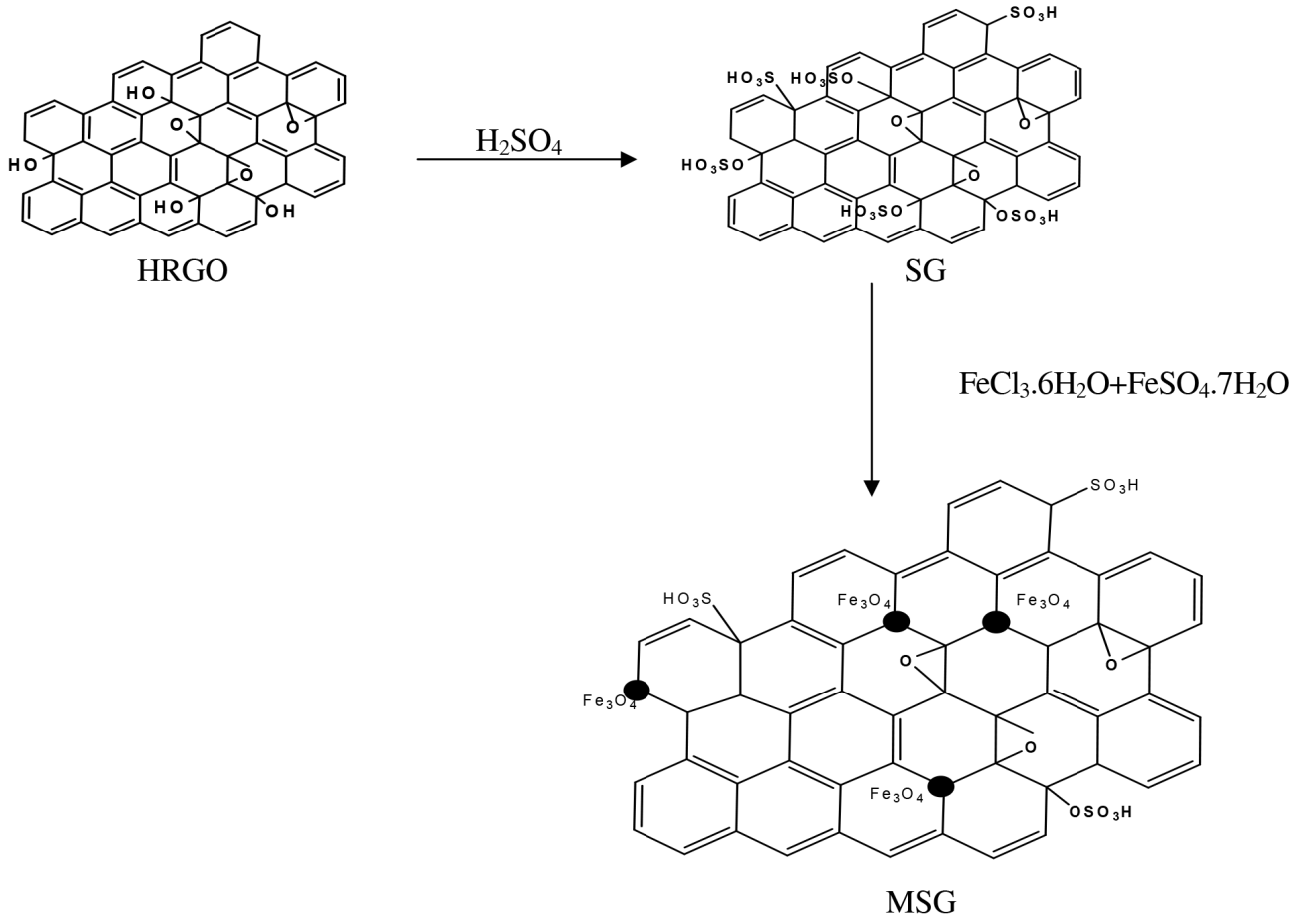


Fig. 1. Proposed scheme for the formation of SG and MSG.

ratio [$Fe^{2+}$]:[$Fe^{3+}$] equal to 1:2, corresponding to $Fe_3O_4$, were dispersed using an ultrasonic dispersion method into 60 mL 1:1 (volume ratio) water–ethanol mixed solvents. The mixture was then poured rapidly into a four-neck bottle under vigorous mechanical stirring for 10 min with $N_2$ bubbling throughout the reaction. The nanocomposites were separated magnetically, washed with deionized water until the throw-down solution became neutral, and were dried in a vacuum oven at 80°C for 12 h.

### 2.3. Acid groups content and zeta potential measurement

The content of acid groups was determined by acid–base titration for SG and MSG, where 0.5 g of SG or MSG was sonicated in 50 mL of 1 M NaCl for 24 h. The suspension was titrated slowly with 0.01 M NaOH solution to reach the neutral point (pH 7) and was monitored using phenolphthalein as an indicator.

The equivalent weight (EW) was calculated using Eq. (1) as follows:

$$\mathrm{EW} = \frac{W}{V_{\mathrm{NaOH}} \times C_{\mathrm{NaOH}}} \quad (1)$$

where $V_{\mathrm{NaOH}}$ and $C_{\mathrm{NaOH}}$ are the volume and concentration of NaOH solution used in the titration and $W$ is the dry weight of SG or MSG samples. The equivalent weight (EW) for SG and MSG was found to be 0.7 and 0.37 g $mol^{-1}$.

For zeta potential measurements, 0.05 g of HRGO, SG or MSG was added into 10 mL of 1 M NaCl solutions. Before zeta potential measurements, all samples were sonicated for 10 min. The zeta potential was determined using a Malvern Nanosizer zeta potential and pH of the suspensions was adjusted using 0.1 M NaOH or HCl.

### 2.4. Characterization of functionalized graphene materials

X-ray diffraction (XRD) data (Shimadzu-7000, USA) was collected with a CuK$\alpha$ radiation beam ($\lambda$ = 0.154060 nm). Fourier transform infrared (FTIR) analysis was conducted using a Bruker ALFA FTIR spectrometer, (USA) with a range from 400 to 4,000 $cm^{-1}$. A transmission electron microscope (TEM) (TECNAI G20, Netherland with energy dispersive X-Ray spectroscopy)was also used. Elemental analysis was conducted using a vario-Micro CHN elemental analyzer (Germany). The Brunauer–Emmett–Teller (BET) surface area and total pore volume were measured using Barrett–Joyner–Halenda (BJH) adsorption methods.

*2.5. Adsorption tests*

The adsorption tests were conducted using a batch equilibration technique by adding a specific weight of prepared adsorbent materials to 50 mL of Cd(II) and Pb(II) solutions at 25°C using a thermostated shaker at 150 rpm. Different initial concentrations of metal solutions (50, 100, 150 and 200 mg $L^{-1}$) were prepared by dilution of 1 g $L^{-1}$ stock solutions of $Cd(NO_3)_2{\cdot}4H_2O$ or $Pb(NO_3)_2$ with deionized water. After the adsorption processes, the solid and liquid phases were separated by centrifuging at 3,600 rpm for 10 min for HRGO and SG adsorbent while a permanent magnet was used for MSG adsorbent. The residual metal concentration in the solution was determined using Inductive Coupled Plasma Mass Spectrometer (ICP-MS, Agilent 7700, USA).

The adsorbed metal amounts were determined using the following formulas [34]:

$$q_t = \frac{(C_0 - C_t)}{m} V \tag{2}$$

$$q_e = \frac{(C_0 - C_e)}{m} V \tag{3}$$

where $q_t$ and $q_e$ (mg $g^{-1}$) are the amounts of the metal adsorbed per unit weight of the adsorbent at time $t$ and equilibrium, $C_0$, $C_t$ and $C_e$ mg $L^{-1}$ are the metal concentrations at the initial time, time $t$ and the equilibrium time respectively; $V$ (L) is the volume of metal solution; and $m$ (g) is the weight of the adsorbent. The removal efficiency ($R$ %) was calculated as follows:

$$R\% = \frac{(C_0 - C_t)}{C_0} \times 100 \tag{4}$$

The distribution coefficient ($K_d$) of Cd(II) and Pb(II) onto different prepared adsorbent was calculated using the following equation [35]:

$$K_d = \frac{q_e}{C_e} \tag{5}$$

A selectivity coefficient ($\alpha$) for the binding of a particular adsorbate in the presence of interfering ions was calculated using the following equation [36]:

$$\alpha = \frac{K_d(\mathrm{T})}{K_d(\mathrm{I})} \tag{6}$$

where $K_d$ (T) is the $K_d$ value of the targeted metal as lead and $K_d$ (I) is the $K_d$ value of the other metal in the multi-metal solutions as cadmium.

To optimize the conditions for removing Cd(II) and Pb(II), a relationship between factors and responses using the response surface methodology models was established. The design matrix follows Box–Behnken design [37] with 13 trials using three factors: $X_1$ (time; min), $X_2$ (metal initial concentration; mg $L^{-1}$), and $X_3$ (adsorbent dose; mg) at three levels (−1, 0, and 1) were chosen to estimate the performance of the adsorption process [38]. Data analysis and optimization were conducted using the statistical software "Statistica". After optimization of the adsorption process by response optimizer, the kinetic and isotherm parameters were investigated.

Considering the competition of both cations, the effect of co-existing of the two metal ions in wastewater on the adsorption process was explored.

*2.6. Kinetics of adsorption process*

The rate and mechanism of the adsorption process could be elucidated based on kinetic studies with different initial concentrations of Cd(II) and Pb(II) varied from 50 to 200 mg $L^{-1}$. For kinetic studies, the pH was fixed at 5.5 (avoiding precipitate with hydroxyl) and adsorption time was varied from 1 to 30 min and dose of adsorbent; 0.02 mg $mL^{-1}$. In order to elucidate the adsorption kinetics, the pseudo-first-order and pseudo-second-order models were applied [12,31].

$$q_t = q_e\,[1 - \exp(-k_1 t)] \tag{7}$$

$$q_t = \frac{k_2 q_e^2 t}{1 + k_2 q_e t} \tag{8}$$

where $k_1$ and $k_2$ are pseudo-first-order and pseudo-second-order adsorption rate constants, respectively.

The pseudo-first-order kinetic model is more suitable for low concentration of solute. It can be written in the following form [31]:

$$\ln(q_e - q_t) = \ln q_e - k_1 t \tag{9}$$

where $q_e$ is the amount of metal adsorbed at saturation per gram of adsorbent (mg $g^{-1}$), $q_t$ is the amount of metal adsorbed at time $t$ per gram of adsorbent (mg $g^{-1}$), and $k_1$ ($min^{-1}$) is the rate constant of the pseudo-first-order adsorption. While, the pseudo-second-order kinetic model is dependent on the solute amount adsorbed on the surface of adsorbent and the adsorbed amount at equilibrium.

To test the diffusion mechanism of Cd(II) and Pb(II) onto prepared graphene-based adsorbents, an intra-particle diffusion model was used at different initial concentrations in the following form [31]:

$$q_t = k_i\, t^{1/2} + C \tag{10}$$

where $k_i$ (mg $g^{-1}$ $min^{-1/2}$) is the intra-particle diffusion rate constant which is the slope of the straight line of $q_t$ vs. $t^{1/2}$ and $C$ is the value of intercept which is a constant reflecting the significance of the boundary layer or mass transfer effect.

*2.7. Sorption isotherms*

The adsorption thermodynamics and isotherms were tested to validate the metal uptake behaviour of the HRGO, SG, and MSG using Langmuir and Freundlich isotherms. The sorption capacity of the prepared material at different initial concentrations at equilibrium can be illustrated by the adsorption isotherms. Adsorption isotherms describe how the adsorbate interacts with adsorbents and give a thorough understanding of the nature of interaction. Several isotherm

equations have been developed and employed for such analysis and the two important isotherms were applied.

*2.7.1. Langmuir isotherm model*

Langmuir's isotherm was used for monolayer adsorption on a surface containing a finite number of identified sites with negligible interaction between adsorbed molecules and assumes uniform energies of adsorption on the surface. In addition the maximum adsorption depends on the saturation level of monolayer. The Langmuir isotherm is represented by the following linear equation:

$$\frac{q_e}{C_e} = \frac{1}{K_L q_m} + \frac{C_e}{q_m} \tag{11}$$

where $q_e$ is the solid-phase concentration in equilibrium with the liquid-phase concentration $C_e$ expressed in mole $L^{-1}$, $q_m$ is the maximum monolayer adsorption capacity (mg $g^{-1}$), and $K_L$ is an equilibrium constant (L $mol^{-1}$). A straight line with slope of $1/q_m$ and intercept of $1/q_m K_L$ is obtained when $C_e/q_e$ is plotted against $C_e$. The separation factor ($R_L$) is a dimensionless constant which is an essential characteristic of the Langmuir model. The equation of $R_L$ is expressed as:

$$R_L = \frac{1}{(1 + k_L C_0)} \tag{12}$$

where $C_0$ (mg $L^{-1}$) is the highest studied initial concentration, ($C_0$ = 150 mg $L^{-1}$). $R_L$ indicates if the isotherm is unfavorable when $R_L > 1$, linear at $R_L = 1$, favorable at $0 < R_L < 1$, or irreversible at $R_L = 0$.

*2.7.2. Freundlich isotherm model*

Adsorbents that follow the Freundlich isotherm equation are assumed to have a heterogeneous surface consisting of sites with different adsorption potentials, and each type of site is assumed to adsorb molecules, as in the Langmuir equation:

$$\ln q_e = \ln K_f + \frac{1}{(n \ln C_e)} \tag{13}$$

where $K_f$ is constant (function of energy of adsorption and temperature) and $n$ is a constant related to adsorption intensity, by plotting ln $q_e$ vs. ln $C_e$ which gave a straight line with slope of $1/n$ and intercept of ln $K_f$. The magnitude of the "$n$" shows an indication of the favorability of adsorption.

*2.8. Sorption thermodynamics*

Adsorption thermodynamic experiments were performed with initial concentration of 100 mg $L^{-1}$ at 25°C and 35°C. Thermodynamic parameters were calculated by the following equations [31,34] where $K_D$ is the equilibrium partition constant, $\Delta G$ (kJ $mol^{-1}$) is the Gibbs free energy change, $R$ (8.314 J $mol^{-1}$ $K^{-1}$) is the universal gas constant, $T$ (K) is the temperature, $\Delta H$ (kJ $mol^{-1}$) is the enthalpy change and $\Delta S$ (kJ $mol^{-1}$ $K^{-1}$) is the entropy change.

$$K_D = q_e / C_e \tag{14}$$

$$\Delta G = -RT \ln K_D \tag{15}$$

$$\ln K_D = \left(\frac{\Delta S}{R}\right) - \left(\frac{\Delta H}{RT}\right) \tag{16}$$

The values of $\Delta G$ were calculated from the $K_D$ values for each temperature, the values of $\Delta H$ and $\Delta S$ were calculated from the slope and intercept of the plot of ln $K_D$ vs. $1/T$, respectively.

*2.9. Regeneration and reuse test*

Regeneration and reuse experiments are necessary for evaluating the practical feasibility for an adsorbent. Thus, to investigate the reversibility of metal ion adsorption with MSG, 10 mg of MSG were mixed with 50 mL of 20 mg $L^{-1}$ Cd(II) and Pb(II). The mixture was shaken at 120 rpm for 15 min. Immediately after adsorption process 0.1 M HCl was added and then the solution was ultrasonically treated at room temperature for 15 min; then the adsorbent was separated by an external magnetic field, washed, dried in an oven at 40°C for 2 h and reused. The metal ion concentrations were determined via ICP-MS. Five cyclic adsorption–desorption processes were conducted to study the regenerability.

## 3. Results and discussion

*3.1. Characterization of functionalized graphene materials*

All the samples were subjected to the elemental analysis to determine their composition of samples as shown in supplementary information (Table 1).

To investigate the functional groups of the HRGO, SG, and MSG samples, further investigations were conducted with the FTIR and by comparing the sample of HRGO with the sample of SG as shown in Fig. 2a, additional bands at 839 and 1,090 $cm^{-1}$ were noted. The bands were associated with the S=O bond [39], illustrating the successful grafting of the $SO_3H$ groups onto prepared HRGO and the existence of the band at 1,118 $cm^{-1}$, specified to the S–phenyl vibration [39]. The peak in the MSG sample at 525 $cm^{-1}$ was characteristic of the Fe–O stretching vibration [24] compared with the HRGO and SG. However, the peak at approximately 1,720 $cm^{-1}$ for all samples was assigned to the C=O bond, which referred to the lower-content oxygen atoms on the samples while the broad band assigned to the –OH stretching mode of the hydroxyl groups was centered at approximately 3,440 $cm^{-1}$.

Table 1
Elemental composition and $SO_3H$ contents of SG and MSG

| Elemental composition (wt.%) | SG | MSG |
|---|---|---|
| C | 63.3 | 70.4 |
| S | 5.6 | 3.1 |
| Fe | – | 6.12 |
| O | 31.1 | 20.4 |
| $SO_3H$ contents (mmol $g^{-1}$) | 0.7 | 0.37 |

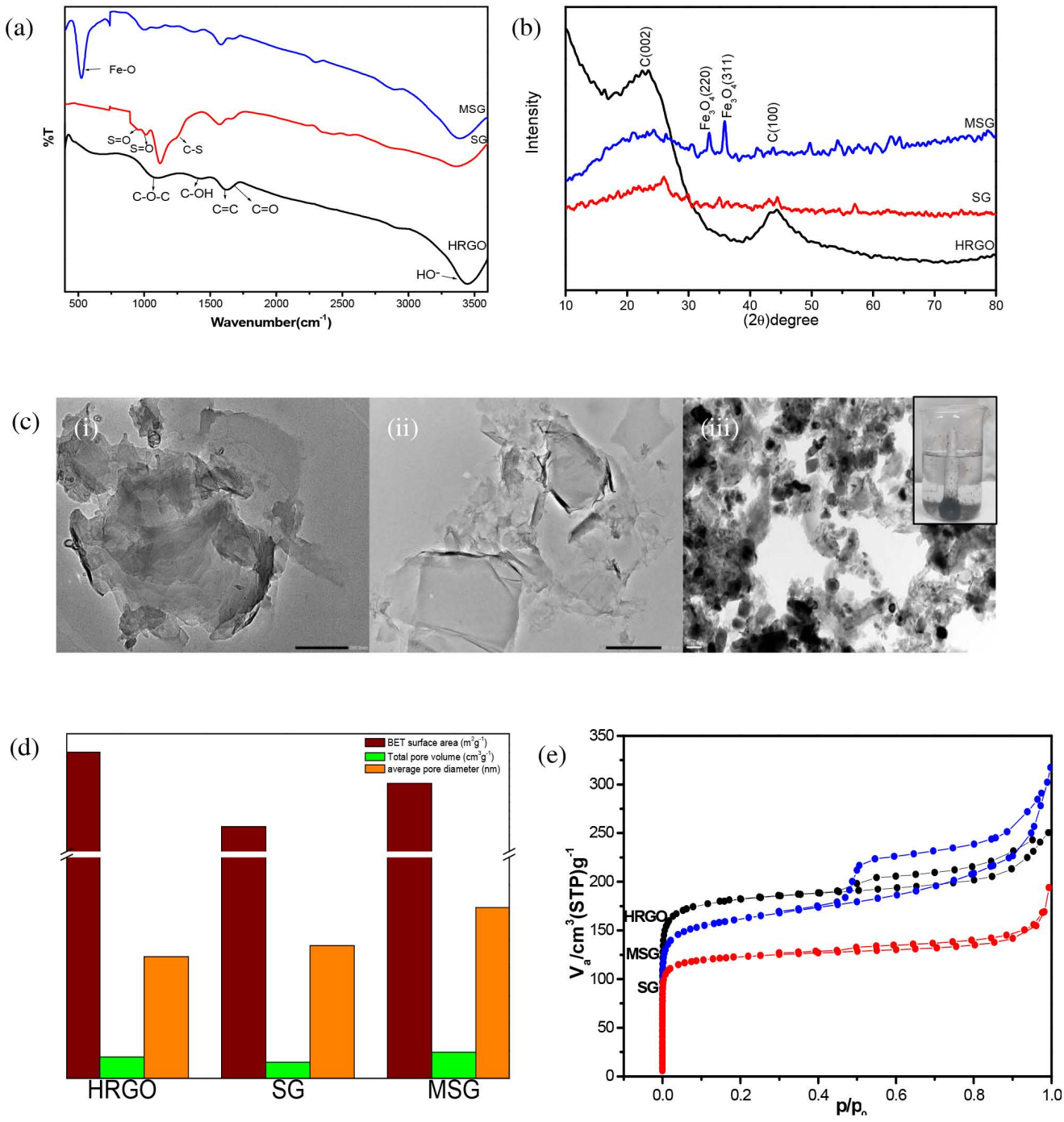


Fig. 2. (a) FTIR, (b) XRD, (c) TEM images (i) HRGO, (ii) SG, (iii) MSG, (d) comparable chart for BET surface area, average pore diameter and total pore volume of HRGO, SG, and MSG and (e) $N_2$ adsorption–desorption isotherms for the prepared graphene materials at 77 K.

In the powder XRD pattern of prepared samples (Fig. 2b), the main peak at 26° and 44.3° 2θ corresponds to the (002) and (100) reflections for HRGO. The reappearance of a broadened weak peak at approximately 2θ = 26° for the SG sample was attributed to limited ordering of a few layers and the irregular interlayer spacing over the whole sample [14,40]. For MSG, due to $Fe_3O_4$ nanoparticles between the MSG nanosheets, a slight decrease in 2θ occurred followed by an increase in interlayer spacing [41,42]. The peaks at 2θ values of 30.28 (220), 35.78 (311), 53.78 (422), 57.18 (511), and 62.88 (440) were consistent with the standard XRD data for the cubic face-centered structure of $Fe_3O_4$ phase (JCPDS card: 19-0629), which indicated the existence of $Fe_3O_4$ in the MSG sample.

As shown in Figs. 2c-i and c-ii, the TEM images of HRGO and SG nanosheets demonstrate an exfoliated, randomly aggregated, crumpled, transparent flake-like morphology with several layers. While, the TEM image of MSG (Fig. 2c-iii) shows entrapped well-dispersed magnetite nanoparticles inside the SG matrix. The left inset in Fig. 2c-iii shows that MSG could be homogeneously dispersed into an aqueous solution and separated by an external magnet, and that the clear solution could be easily removed.

BET analysis was used to investigate the specific surface area of different samples. The results of analyzing the surface area and the pore volume of all samples by nitrogen adsorption–desorption isotherms are illustrated in Table 2. As shown in Fig. 2e, the isotherm curves of all samples were elucidated as type-IV isotherms according to IUPAC classification [43] with distinct hysteresis loops in the range of relative pressures ($P/P_0$) from 0.45 to 1.0, indicating existence of mesopores. The surface area and the pore volume of SG were slightly lower than that of HRGO, which had a partially damaged porous structure from the sulfonation process.

The pore size distributions of prepared graphene-based materials are shown in Fig. 3. All samples contain micropores with size less than 2 nm in addition to many mesopores with size ranged between 2 and 20 nm whereas the mesopores structure can facilitate the ion diffusion.

### 3.2. Surface chemistry and the effect of solution pH

As shown in Fig. 4a, the zeta potential of the prepared materials was investigated and it was noted that as pH increased from 3 to 9, the zeta potential values of HRGO, SG, and MSG decreased due to the surfaces of HRGO, SG, and MSG being highly oxidized with a large number of oxygen functionalities as sulfonic, carboxylic, and hydroxyl groups and that in turn makes the graphene-based adsorbents more suitable for the adsorption process of heavy metal cations in all environmental pH conditions [3]. The zeta potential of SG was lower than that of HRGO and MSG over the whole pH range, which may return to its higher content of sulfonic groups and thus, stabilization of colloidal particles occurs and that would make SG hard to separate from water.

Table 2
Texture feature (surface area, pore volume, and size) for HRGO, SG, and MSG

| | HRGO | SG | MSG |
|---|---|---|---|
| BET surface area ($m^2 g^{-1}$) | 702 | 475 | 607 |
| Total pore volume ($cm^3 g^{-1}$) | 0.386 | 0.288 | 0.469 |
| Average pore diameter (nm) | 2.2 | 2.4 | 3.09 |

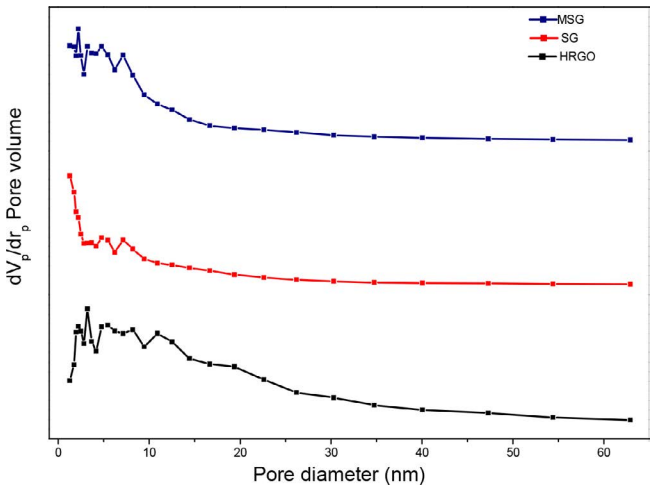


Fig. 3. Pore size distribution of HRGO, SG, and MSG calculated using DFT method.

The solution pH is one of the important parameters controlling the adsorption process, and it affects the interaction between the adsorbate and the charges on the adsorbent surface. For this reason, the influence of solution pH on the adsorption efficiency of HRGO, SG and MSG toward Cd(II) and Pb(II) was evaluated in the range from 3 to 9 to determine the optimal pH value. As shown in Figs. 4b and c, the removal efficiency dramatically increased when the pH was increased from 4 to 7. However, when the solution was in the range of 7–8, the removal efficiency had slow progress. Once pH went beyond 8, the adsorption amount was decreased. Many reasons could explain Cd(II) and Pb(II) adsorption behaviour on the prepared adsorbents relative to the pH values. For instance, at low pH values (less than 4), the surfaces of HRGO, SG, and MSG would be surrounded by numerous hydronium ions that compete with metal ions. On the other hand, by increasing solutions pH the electrostatic repulsion between the metal ions and the surface of the adsorbent is reduced; therefore, the removal efficiency is gradually increased. However at a pH slightly below 6, MSG showed a higher tendency of removing Cd(II) and Pb(II) more than HRGO and SG. This could be due to the electronic density of the MSG surface caused by the $Fe_3O_4$ addition which would prompt low bonding energy with Cd(II) and Pb(II) due to its oxidized surface. Conversely, a relative repulsion could occur at a pH of 6, which would be possible due to the $Fe_3O_4$ on MSG surface at that pH having a net positive charge (the point of zero charge of $Fe_3O_4$ is between 6 and 6.4) [44]. Therefore, a pH of 5.5 was selected as the optimum pH for removing Cd(II) and Pb(II) in the other experiments.

On the other hand, Cd(II) and Pb(II) exist in various forms at different pH as, when the pH is greater than 7, hydroxide precipitates can be easily formed and it would be difficult to be adsorbed onto the negatively charged surface of the adsorbent due to electrostatic repulsion. Thus, the concentrations of the Cd(II) and Pb(II) ions dramatically decrease at pH more than 8 because $Cd(OH)_2$ and $Cd(OH)_3^-$ begin to form [3], in the same time with $Pb(OH)_2$ and $Pb(OH)_3^-$ which are difficult to be removed by the adsorbent.

### 3.3. Competitive adsorption

Essentially, the distribution coefficient ($K_d$) represents the true performance of an adsorbent according to the ratio of adsorption capacity of adsorbent to final concentration of adsorbate in the liquid at equilibrium [34,35] while, the adsorption capacity and removal efficiency can be altered by the operating conditions. Distribution coefficient ($K_d$) was used to evaluate the effectiveness of different prepared adsorbent materials in this study using Eq. (5) (Table 3) and

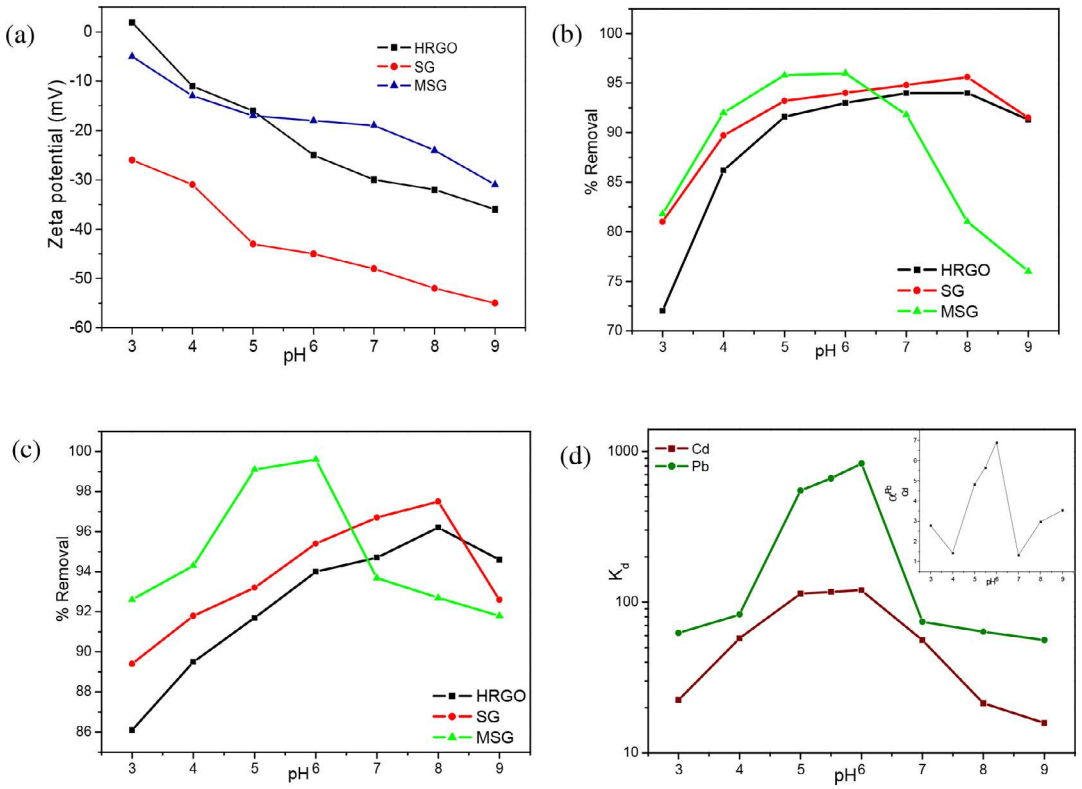


Fig. 4. (a) Zeta potential of HRGO, SG, and MSG, and effect of solution pH on the removal of (b) Cd(II), (c) Pb(II) adsorbed onto HRGO, SG, and MSG (Experimental conditions: $C_0$: 100 mg $L^{-1}$; dose of adsorbent: 0.2 mg $mL^{-1}$; temperature: 25°C; time: 30 min; volume: 50 mL), (d) effect of pH on distribution coefficient for Cd(II) and Pb(II) adsorbed onto MSG and the inset is the selectivity coefficient of MSG for Pb(II) to Cd(II) in the multi-metal solutions.

Table 3
Performance metrics of the prepared nanomaterials used for Cd(II) and Pb(II) removal at pH 5.5 and 100 mg $L^{-1}$ metal initial concentration

| | Maximum adsorption capacity (mg $g^{-1}$) | | Maximum removal efficiency (%) | | Distribution coefficient (L $g^{-1}$) | |
|---|---|---|---|---|---|---|
| | Cd(II) | Pb(II) | Cd(II) | Pb(II) | Cd(II) | Pb(II) |
| HRGO | 462 | 464 | 92 | 93 | 60 | 65 |
| SG | 468 | 472 | 94 | 94 | 73 | 83 |
| MSG | 480 | 497 | 96 | 100 | 117 | 764 |

analyze the selectivity of MSG for Pb(II) to Cd(II) in the multi-metal solutions using Eq. (6) as shown in the inset of Fig. 4d and compare the distribution coefficient values with others from previous studies as illustrated in Table 4 [27,36,45–49].

As shown in Fig. 4d, with increasing pH an increase in $K_d$ values for Cd(II) and Pb(II) occurred due to increasing pH activate more adsorption sites and more metal ions were available to migrate from the solution to the surface of the MSG. In addition, MSG showed more prominent selectivity for Pb(II) over Cd(II) at each pH value. According to selectivity coefficient values and single metal adsorption onto MSG, Pb(II) presented great affinity for MSG in the single- and the multi-metal system, indicating that MSG had selective adsorption for Pb.

### 3.4. Optimization of Cd(II) and Pb(II) adsorption

An optimization of the adsorption processes was achieved using Box–Behnken design with three variables, time (min), metal initial concentration (mg $L^{-1}$), and adsorbent dose (mg), as illustrated in Table 5 for Cd(II) and Pb(II) on MSG. The solution pH values during the whole reaction time were kept constant at pH 5.5.

The statistical relationship between variables and responses was explained using quadratic model in terms of coded factors in the following equations:

$$Y_{Cd(II)} = 92 + 6.5375X_1 - 5.275X_2 + 8.4125X_3 - 4.0375X_1^2 + 0.6875X_2^2\ 7.3375X_3^2 + 1.65X_1X_2 + 3X_2X_3 + 0.975X_1X_3 \quad (17)$$

Table 4
A review of the performance of some carbon-based adsorbent materials used to remove Cd(II) and Pb(II) from water

| Adsorbent nanomaterials | Adsorbate | Optimum adsorption condition (temperature (°C), pH) | Adsorbate initial concentration (mg $L^{-1}$) | Maximum adsorption capacity (mg $g^{-1}$) | Adsorbate final concentration (mg $L^{-1}$) | Distribution coefficient (L $g^{-1}$) | References |
|---|---|---|---|---|---|---|---|
| Chitosan-pyromellitic dianhydride modified biochar (CPMB) | Cd(II) | 25, 5 | 500 | 30.12 | 470 | 0.06 | [35] |
| | Pb(II) | | | 9.24 | 491 | 0.02 | |
| Hydrated manganese oxide biochar nanocomposite (HMO-BC) | Cd(II) | 25, 6 | – | 22.3 | 34 | 0.66 | [44] |
| | Pb(II) | | | 67.9 | 58 | 1.2 | |
| Magnetic graphenes composite material ($Fe_3O_4$-GS) | Cd(II) | 25, 7 | 5 | 27.83 | 0.57 | 49 | [45] |
| | Pb(II) | | | 27.95 | 0.59 | 47 | |
| Poly3-aminopropyltriethoxysilane oligomer-linked graphene oxide composite (PAS-GO) | Pb(II) | 30,5 | 400 | 312.5 | 87.5 | 3.6 | [46] |
| Magnetic ethylene diamine-functionalized graphene oxide (MDFGO) | Cd(II) | 25, 6.2 | 50 | 142 | 3 | 47 | [26] |
| | Pb(II) | | | 145 | 2 | 73 | |
| Magnetic graphene oxide/MgAl-layered double hydroxide nanocomposite | Cd(II) | 25, 6 | 300 | 45.05 | 142 | 0.3 | [47] |
| | Pb(II) | | 1,000 | 192.31 | 327 | 0.6 | |
| Sulfanilic acid functionalized graphene oxide (SGO) | Pb(II) | 25,7 | 30 | 454.54 | 11.8 | 38 | [48] |
| Reduced sulfonated graphene oxide (rSGO) | | | | 400 | 14 | 29 | |
| Graphene oxide (GO) | | | | 303.03 | 18 | 17 | |
| Reduced graphene oxide (rGO) | | | | 140.84 | 24 | 6 | |
| MSG | Cd | 25, 5.5 | 100 | 840 | 4 | 210 | This work |
| | Pb | | 100 | 926 | 0.9 | 1,029 | This work |

$$Y_{Pb(II)} = 99.1 + 0.3625X_1 - 2.925X_2 + 4.6875X_3 - 0.0625X_1^2 - 1.6375X_2^2\ 3.1625X_3^2 + 0.45X_1X_2 + 3.25X_2X_3 + 0.175X_1X_3 \quad (18)$$

where $Y$ is the response (yield of removal) and $X_1$, $X_2$, and $X_3$ are contact times, initial metal concentration, and adsorbent dose, respectively.

As shown in Fig. 5, the 3D surface plots, which present the results of the Box–Behnken design, show the type of interaction between the tested variables, which display the optimum conditions. It was observed that the removal efficiency decreased with an increase in initial metal concentrations from 50 to 150 mg $L^{-1}$ while it increased by increasing the contact time and then remained approximately constant. This observation revealed that in the beginning, the metal ions were adsorbed externally and the adsorption rate increased rapidly. When the external surface became saturated, the metal ions adsorbed into the porous structure of the adsorbent and finally reached a constant value where no more adsorption occurred.

To remove Cd(II) completely according to the solved equation, the optimal levels of the three components at the maximum point of the polynomial model were 13.28 min contact time, 50 mg $L^{-1}$ of Cd(II) concentration, and 0.012 mg of MSG at a pH of 5.5°C and 25°C. However, at contact time 2.9 min, 100.7 mg $L^{-1}$ of Pb(II) and 0.14 mg of MSG complete removal was achieved. A confirmation test (three replicate) took place by using statistical analysis condition which provide 99.5% removal for Cd(II) and 99.8% removal for Pb(II).

Table 5
Central composite matrix of experimental and predicted values for Cd(II) and Pb(II) removal (%) using prepared MSG at solutions pH 5.5

| Trial | Time ($X_1$; min) | Adsorbate initial concentration ($X_2$; mg $L^{-1}$) | Adsorbent dose ($X_3$; mg) | Removal (%) | | | |
|---|---|---|---|---|---|---|---|
| | | | | Measured | | Predicted | |
| | | | | Cd(II) | Pb(II) | Cd(II) | Pb(II) |
| 1 | 10 | 50 | 0.005 | 86.8 | 96 | 75.1 | 92.1 |
| 2 | 10 | 150 | 0.005 | 69.4 | 82.1 | 69.4 | 91.4 |
| 3 | 10 | 50 | 0.015 | 95.3 | 100 | 96 | 98.1 |
| 4 | 10 | 150 | 0.015 | 89.9 | 99.1 | 77 | 93.9 |
| 5 | 5 | 50 | 0.01 | 89 | 99.1 | 82.3 | 96 |
| 6 | 5 | 150 | 0.01 | 76 | 93.9 | 86.8 | 96.6 |
| 7 | 15 | 50 | 0.01 | 98 | 100 | 89 | 99.1 |
| 8 | 15 | 150 | 0.01 | 91.6 | 96.6 | 89.9 | 99.1 |
| 9 | 5 | 100 | 0.005 | 65.1 | 92.1 | 91.6 | 99.1 |
| 10 | 5 | 100 | 0.015 | 82.3 | 100 | 92 | 100 |
| 11 | 15 | 100 | 0.005 | 77 | 91.4 | 95.3 | 100 |
| 12 | 15 | 100 | 0.015 | 98.1 | 100 | 98 | 100 |
| 13 | 10 | 100 | 0.01 | 92 | 99.1 | 98.1 | 100 |

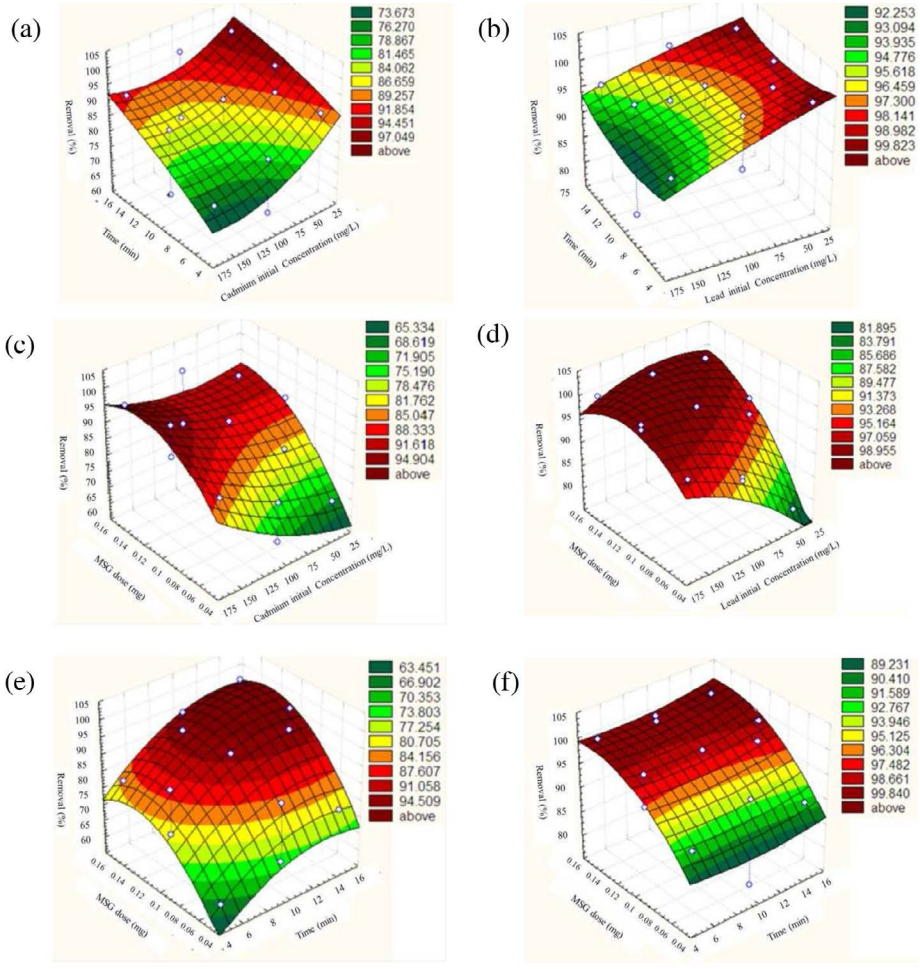


Fig. 5. Response surface plots for removal efficiency (%) of Cd(II) and Pb(II) on MSG.

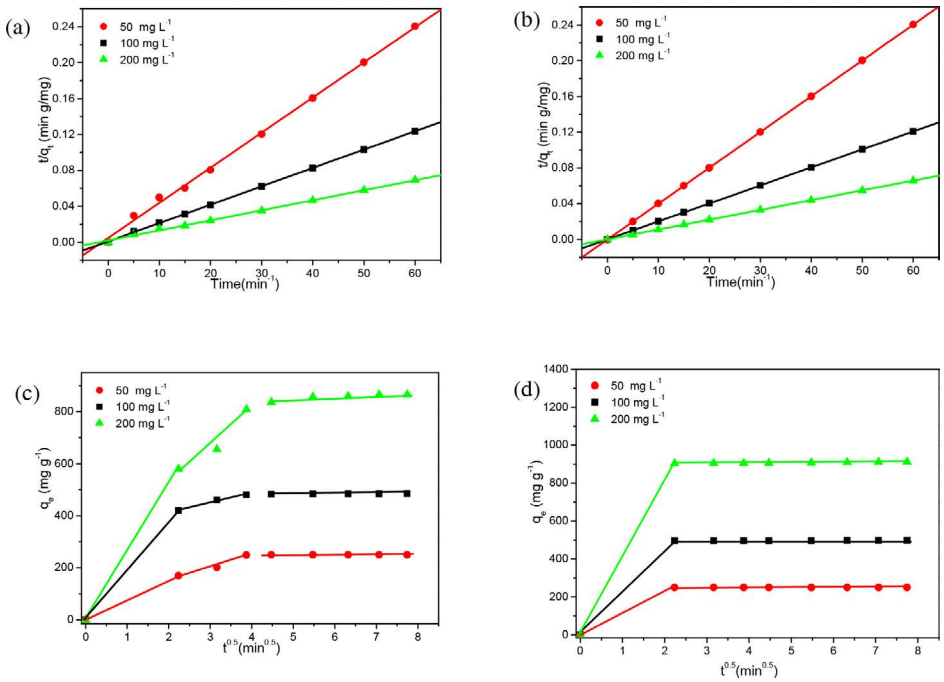


Fig. 6. Pseudo-second-order and intra-particle diffusion kinetic models for the adsorption of cadmium on MSG (a) and (c) respectively and lead (b) and (d) (conditions: dose of adsorbent; 0.02 mg mL$^{-1}$, temperature; 25°C).

### 3.5. Adsorption kinetic models

The pseudo-first-order and the pseudo-second-order models were two kinetic models used to test the effect of varying the adsorption time on the rate of the adsorption process (Fig. 6).

These models were helpful in understanding the adsorption mechanism of Cd(II) and Pb(II) at various initial concentrations (50, 100, and 200 mg L$^{-1}$) using the prepared MSG adsorbent.

The pseudo-first-order presumed that the adsorption capacity was restricted by only one mechanism acting on one class of adsorbing sites [50]. By comparing the experimental adsorption capacities with the calculated capacities values, it was found that the calculated values were far from their comparable experimental values. Therefore, the pseudo-first-order reaction kinetic model was not adequate to depict adsorption of Cd(II) and Pb(II) on MSG.

Conversely, the pseudo-second-order kinetic model was dependent on the adsorbate amount adsorbed on the surface of the adsorbent and the adsorbed amount at equilibrium. As illustrated in Table 6, the calculated $q_e$ values ($q_{e,\text{cal}}$) agreed with the experimental $q_e$ values ($q_{e,\text{exp}}$) and the correlation coefficient ($R^2$) values obtained were consistently higher than those of the pseudo-first-order. From the previous results, the adsorption perfectly obeyed the pseudo-second-order model which meant the controlling rate step was chemisorption and the rate of adsorption for both ions depended on the accessibility to adsorption sites on the surface of adsorbent materials. Moreover, as initial concentrations of Cd(II) or Pb(II) increased, the $k_2$ values decreased, which may be attributed to higher competition for the adsorption sites at high concentrations compared with low concentrations [48].

In order to further research in the diffusion mechanism of Cd(II) and Pb(II) onto MSG, an intra-particle diffusion model was used at different initial concentrations. As shown in Fig. 6c, the adsorption mechanism for Cd(II) into MSG was basically divided into three steps: external diffusion of the adsorbate from the aqueous solution to the surface of the adsorbent, followed by gradual adsorption step from the adsorbent surface to inside the pores and lastly, the final equilibrium step whereas an adsorption reaction occurred with the functional groups within the pores. However, the adsorption rate mainly depended on the first two processes which most likely depend on electrostatic interactions and it is a rapid interaction, therefore the rapid removal of cadmium occurred. On the other hand, the intra-particle diffusion of Pb(II) as shown in Fig. 6d could be almost divided into two steps, a rapid initial step which represents the diffusion of Pb(II) from solution to the surface of MSG followed by a relatively slow step which explains the macropore and mesopore diffusion of ions into MSG with controlling intra-particle diffusion [50].

### 3.6. Adsorption isotherms

By using Langmuir and Freundlich adsorption isotherm models [49,51] at different initial concentrations and two different temperatures (25°C and 35°C), as illustrated in Table 7, it could be concluded that the Langmuir model best represented the adsorption data suggesting that Cd(II) and Pb(II) ions adsorption is monolayer coverage and the maximum value $q_m$ of Cd(II) ions adsorption on MSG is 901 mg g$^{-1}$ while for Pb(II) ions is 926 mg g$^{-1}$and the adsorption behaviour was more effective at high temperatures. Furthermore, for the Freundlich model, the values of $1/n_F$, which measure the adsorption intensity or surface heterogeneity, fluctuated between 0 and 1, which elucidated a greater heterogeneity as the values

Table 6
Parameters and determination coefficients of the kinetic models for Cd(II) and Pb(II) adsorption on prepared MSG

| | Cd(II) initial concentrations (mg $L^{-1}$) adsorbed on MSG | | | Pb(II) initial concentrations (mg $L^{-1}$) adsorbed on MSG | | |
|---|---|---|---|---|---|---|
| | 50 | 100 | 200 | 50 | 100 | 200 |
| $q_{e,exp}$ (mg $g^{-1}$)[a] | 250 | 489 | 866 | 250 | 497 | 913 |
| Pseudo-first-order | | | | | | |
| $q_{e,cal}$ (mg $g^{-1}$) | 22 | 47 | 751 | 0.26 | 3.2 | 22 |
| $k_1$ ($min^{-1}$) | 0.12 | 0.1 | 0.15 | 0.02 | 0.05 | 0.06 |
| $R^2$ | 0.8 | 0.95 | 0.97 | 0.94 | 0.91 | 0.83 |
| Pseudo-second-order | | | | | | |
| $q_{e,cal}$ (mg $g^{-1}$) | 255 | 488 | 893 | 250 | 497 | 909 |
| $k_2$ ($min^{-1}$) | 0.003 | 0.0005 | 0.0006 | 0.98 | 0.07 | 0.01 |
| $R^2$ | 0.99 | 0.99 | 0.99 | 1 | 1 | 0.99 |

[a]Equilibrium time for cadmium removal was equal to 15 min, while for lead removal it was equal to 5 min.

Table 7
Adsorption isotherm parameters for the adsorption of Cd(II) and Pb(II) on prepared MSG; adsorbent dosage 0.02 mg $mL^{-1}$

| | Cd(II) adsorption on MSG | | Pb(II) adsorption on SG | |
|---|---|---|---|---|
| Temperature °C | 25°C | 35°C | 25°C | 35°C |
| Langmuir isotherm | | | | |
| $q_m$ (mg $g^{-1}$) | 840 | 901 | 926 | 926 |
| $K_L$ (L $mg^{-1}$) | 0.5 | 0.7 | 0.75 | 0.74 |
| $R^2$ | 0.998 | 0.997 | 0.999 | 0.999 |
| $R_L$ | 0.009 | 0.007 | 0.007 | 0.007 |
| Freundlich isotherm | | | | |
| $K_F$ (mg $g^{-1}$) | 220 | 216 | 228 | 232 |
| $1/n_F$ | 0.22 | 0.21 | 0.24 | 0.21 |
| $R^2$ | 0.999 | 0.997 | 0.995 | 0.993 |

Table 8
Thermodynamic parameters for adsorption of 100 mg $L^{-1}$ Cd(II) and Pb(II) on MSG at 25°C and 35°C

| | $T$ (K) | $\Delta H$ (kJ $mol^{-1}$) | $\Delta S$ (J $mol^{-1}$ $K^{-1}$) | $\Delta G$ (kJ $mol^{-1}$) |
|---|---|---|---|---|
| Cd(II) | 298 | 3.06887 | 39.49851 | –11,862 |
| | 308 | | | –13,205.3 |
| Pb(II) | 298 | 3.50338 | 52.1216 | –15,636.6 |
| | 308 | | | –17,240.4 |

approached zero. It was also concluded that, a heterogeneous chemisorption process occurred and that is in good agreement with the intra-particle diffusion kinetics and the fact that Cd(II) and Pb(II) ions sorbed onto MSG mainly through inner surface with controlling intra-particle diffusion. In conclusion, the results indicate that the adsorption of both metals is effective using Langmuir and Freundlich isotherm models.

### 3.7. Adsorption thermodynamics

Thermodynamic parameters such as Gibbs free energy ($\Delta G$), enthalpy ($\Delta H$), and entropy ($\Delta S$) were explored at 25°C and 35°C and listed in Table 8. The negative values of $\Delta G$ showed that Cd(II) and Pb(II) adsorbent systems were spontaneous [52] and this character increases as the temperature increases. The positive values of $\Delta H$ indicate an endothermic nature of the adsorption process, while the positive values of $\Delta S$ indication for randomness increasing in the solid–liquid interface during the adsorption process [31]. Above all, it was concluded that the adsorption of Cd(II) and Pb(II) on the MSG is an endothermic, randomness and spontaneous process.

### 3.8. Speculation of adsorption mechanism

It was proposed that the adsorption of Cd(II) and Pb(II) on HRGO, SG, and MSG was dependent on the functional groups, the surface area, the pore size and pore uniformity in

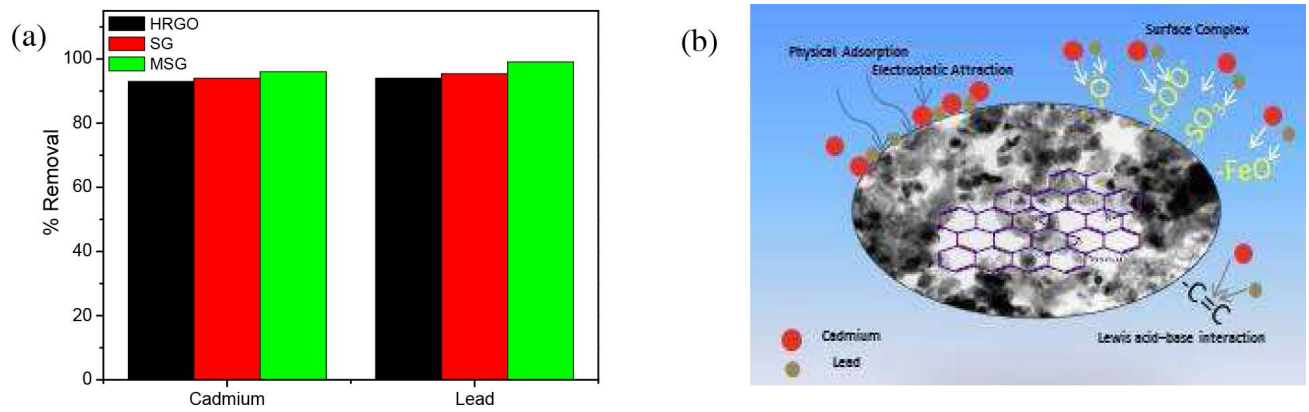


Fig. 7. (a) Comparing the removal percentage of Cd(II) and Pb(II) using the three prepared graphene based adsorbents at pH 5.5, (b) scheme for the adsorption mechanism.

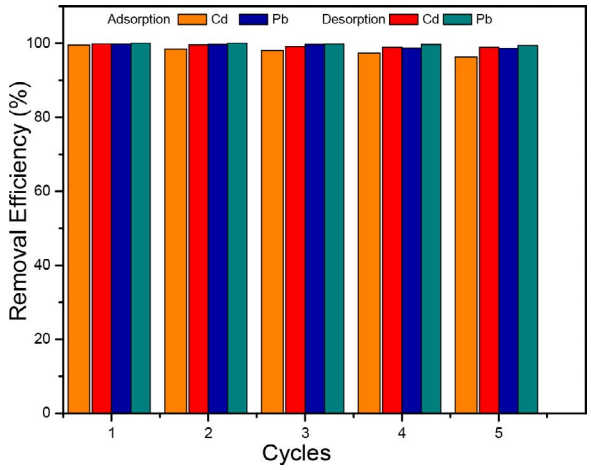


Fig. 8. Adsorption-desorption cycles of Cd(II) and Pb(II) onto MSG ($C_0$; 20 mg $L^{-1}$, adsorbent dose; 0.02 g $L^{-1}$, pH; 5.5, temperature; 25°C).

the adsorbent materials. The prepared HRGO, SG, and MSG typically have very high surface areas, which if exposed to the solution phase, could provide surface sites for rapid and extensive adsorption process (Fig. 7a and Table 3). According to literature, the main adsorption interactions of metal ions on graphene-based nanomaterial surfaces were electrostatic interactions and cation-π bonding. The adsorption capacity of Cd(II) and Pb(II) on HRGO was due to the presence of the –OH and –COOH groups in the plane and when functionalized with a $–SO_3H$ group, the effective sites of HRGO for adsorption increased due to the sulfonic group powerfully attracting positively charged ions. The incorporation of magnetic particles on the surface of SG afford a large number of active sites which is full of negatively charged, that reflect on increasing the interaction between adsorbate and metal ions and hence the adsorption capacity of MSG. In addition, the graphene lattice contains delocalized π electron system which act as Lewis base in aqueous solution and form electron donor acceptor interaction with metals ions which act as Lewis acid [53] and a complex between graphene-based adsorbents and the heavy metal ions can occur through Lewis acid–base interaction [54] which also contributes to Cd(II) and Pb(II) adsorption on SG and MSG.

In summary, the adsorption of Cd(II) and Pb(II) by the graphene-based adsorbents was mainly through: (i) the electrostatic attraction which was the dominant mechanism in adsorption process; (ii) Lewis acid–base interaction between π-electron depleted regions on the surface of graphene and metal cations.

### 3.9. Desorption–adsorption tests

In order to evaluate the regenerability and reuse of MSG which are important factors to estimate the cost effectiveness of the adsorbent, 0.01 g of MSG after adsorption process were dispersed into a solution of 0.1 M HCl and sonicated for 15 min. After that, the adsorbent was washed and reused. After five cycles, the removal efficiency was still high and the variations in the removal percentage were quite small after each desorption as shown in Fig. 8, and that is a good indication for MSG to be used potentially in wastewater application.

## 4. Conclusion

The post-modification method generally encompasses the intricate and harsh steps of the reduction of GO followed by sulfonation of reduced GO. In this study, SG carried massive $SO_3H$ functional groups obtained directly through a simple process, as demonstrated. The method used was low-cost with simple steps and was effective for the preparation of SG and MSG compared with previous methods. According to the results, the porosity and adsorbent surface area, in addition to the functional groups on the adsorbent surface were important factors in determining the adsorption efficiency and the adsorption rate. However, low acetic solutions promoted Cd(II) and Pb(II) adsorption due to the electrostatic interaction and cation-π bonding between adsorbate and adsorbent surface. Optimisation of the experimental results showed the MSG adsorption equilibrium time for a 50 mg $L^{-1}$ of Cd(II) was only 13.28 min, while that for 100.7 mg $L^{-1}$ of Pb(II) was approximately 2.9 min. However, MSG has excellent reusability which nominates it to many potential applications.

In conclusion, the prepared MSG exhibited superior adsorption properties for Cd(II) and Pb(II) in high environmental concentrations as well as in low concentrations. In addition, this material can be used several times with good stability and cost effectiveness.

## Acknowledgments

The author acknowledges the Dean of Scientific Research at King Faisal University for the financial support under Nasher Track (Grant No. 186171).

The authors from the City of Scientific Research and Technological Applications, Alexandria, Egypt would like to acknowledge the financial support for this work with SRTA City 2017-2022 fund plan.

## References

[1] M.A. Khairia, Cadmium removal from aqueous solution by green synthesis zero valent silver nanoparticles with Benjamina leaves extract, Egypt. J. Aquat. Res., 43 (2017) 269–274.
[2] S. Ata, A. Tabassum, I. Bibi, F. Majid, M. Sultan, S. Ghafoor, M. A. Bhatti, N. Qureshi, M. Iqbal, Lead remediation using smart materials. A review, Z. Phys. Chem. (2019) https://doi.org/10.1515/zpch-2018–1205.
[3] K. Chen, J. He, Y. Li, X. Cai, K. Zhang, T. Liu, Y. Hu, D. Lin, L. Kong, J. Liu, Removal of cadmium and lead ions from water by sulfonated magnetic nanoparticle adsorbents, J. Colloid Interface Sci., 494 (2017) 307–316.
[4] M.F. Elkady, E.M. El-Sayed, H.A. Farag, A.A. Zaatout, Assessment of novel synthetized nanozirconium tungstovanadate as cation exchanger for lead ion decontamination, J. Nanomaterials, 2014 (2014) 11 p, http://dx.doi.org/10.1155/2014/149312.
[5] M. Al-Shannag, Z. Al-Qodah, K. Bani-Melhem, M.R. Qtaishatand, M. Alkasrawi, Heavy metal ions removal from metal plating wastewater using electrocoagulation: kinetic study and process performance, Chem. Eng. J., 260 (2015) 749–756.
[6] S. Ye, G. Zeng, H. Wu, C. Zhang, J. Liang, J. Dai, Z. Liu, W. Xiong, J. Wan, P. Xu, M. Cheng, Co-occurrence and interactions of pollutants, and their impacts on soil remediation-A review, Crit. Rev. Environ. Sci. Technol., 47 (2017) 1528–1553.
[7] S. Ye, G. Zeng, H. Wu, C. Zhang, J. Dai, J. Liang, J. Yu, X. Ren, H. Yi, M. Cheng, C. Zhang, Biological technologies for the remediation of co-contaminated soil, Crit. Rev. Biotechnol., 37 (2017) 1062–1076.
[8] J.R. Utrilla, G.P. Joya, M. Sanchezpolo, M.F. Garcia, I.B. Toledo, Removal of nitroimidazole antibiotics from aqueous solution by adsorption/bioadsorption on activated carbon, J. Hazard. Mater., 170 (2009) 298–305.
[9] Y. Cui, Q. Ge, X.Y. Liu, T.S. Chung, Novel forward osmosis process to effectively remove heavy metal ions, J. Membr. Sci., 467 (2014) 188–194.
[10] D. Alidoust, M. Kawahigashi, S. Yoshizawa, H. Sumida, M. Watanabe, Mechanism of cadmium biosorption from aqueous solutions using calcined oyster shells, J. Environ. Manage., 150 (2015) 103–110.
[11] M.S. Mohy Eldin, M.H. Gouda, M.A. Abu-Saied, Y.M.S. El-Shazly, H.A. Farag, Development of grafted cotton fabrics ions exchanger for dye removal applications: methylene blue model, Desal. Wat. Treat., 57 (2016) 22049–22060.
[12] P.N. Diagboya, B.I. Olu-Owolabi, K.O. Adebowale, Synthesis of covalently bonded graphene oxide–iron magnetic nanoparticles and the kinetics of mercury removal, RSC Adv., 5 (2015) 2536–2542.
[13] P.P. Upare, J. Yoon, M.Y. Kim, H. Kang, D.W. Hwang, Y.K. Hwang, H.H. Kung, J. Chang, Chemical conversion of biomass-derived hexose sugars to levulinic acid over sulfonic acid-functionalized graphene oxide catalysts, Green Chem., 15 (2013) 2935–2943.
[14] Z. Wei, Y. Yang, Y. Hou, Y. Liu, X. He, S. Deng, A new approach towards acid catalysts with high reactivity based on graphene nanosheets, Chem. Cat. Chem., 6 (2014) 2354–2363.
[15] M.M. Antunes, P.A. Russo, P.V. Wiper, J.M. Veiga, M. Pillinger, L. Mafra, D.V. Evtuguin, N. Pinna, A.A. Valente, Sulfonated graphene oxide as effective catalyst for conversion of 5-(hydroxymethyl)-2-furfural into biofuels, Chem. Sus. Chem., 7 (2014) 804–812.
[16] F. Liu, J. Sun, L. Zhu, X. Meng, C. Qi, F.-S. Xiao, Sulfated graphene as an efficient solid catalyst for acid-catalyzed liquid reactions, J. Mater. Chem., 22 (2012) 5495–5502.
[17] J. Ji, G. Zhang, H. Chen, S. Wang, G. Zhang, F. Zhang, X. Fan, Sulfonated graphene as water-tolerant solid acid catalyst, Chem. Sci., 2 (2011) 484–487.
[18] H. Li, Y. Wang, Y. Shi, J. Li, L. He, H.Y. Yang, Large scale synthesized sulphonated reduced graphene oxide: a high performance material for electrochemical capacitors, RSC Adv., 3 (2013) 14954–14959.
[19] J., Zhou, Y. Wang, X. Guo, J. Mao, S. Zhang, Etherification of glycerol with isobutene on sulfonated graphene: reaction and separation, Green Chem., 16 (2014) 4669–4679.
[20] P. Gao, D.D. Sun, W.J. Ng, Multifunctional nanostructured membrane for clean water reclamation from wastewater with various Ph conditions, RSC Adv., 3 (2013) 15202–15210.
[21] G. Zhao, L. Jiang, Y. He, J. Li, H. Dong, X. Wang, W. Hu, Sulfonated graphene for persistent aromatic pollutant management, Adv Mater., 23 (2011) 3959–3963.
[22] G. Zhao, J. Li, X. Wang, Kinetic and thermodynamic study of 1-naphthol adsorption from aqueous solution to sulfonated graphene nanosheets, Chem. Eng. J., 173 (2011) 185–190.
[23] H. Li, J. Fan, Z. Shi, M. Lian, M. Tian, J. Yin, Preparation and characterization of sulfonated graphene-enhanced poly (vinyl alcohol) composite hydrogel and its application as dye absorbent, Polymer, 60 (2015) 96–106.
[24] A. Alizadeh, G. Abdi, M.M. Khodaei, Graphene oxide/$Fe_3O_4$/$SO_3H$ nanohybrid: a new adsorbent for adsorption and reduction of Cr(VI) from aqueous solutions, RSC Adv., 7 (2017) 14876–14881.
[25] X. Hu, Y. Liu, H. Wang, A. Chen, G. Zeng, S. Liu, Y. Guo, X. Hu, T. Li, Y. Wang, L. Zhou, S. Liu, Removal of Cu(II) ions from aqueous solution using sulfonated magnetic graphene oxide composite, Sep. Purif. Technol., 108 (2013) 189–195.
[26] S. Wang, J. Wei, S. Lv, Z. Guo, F. Jiang, Removal of organic dyes in environmental water onto magnetic-sulfonic graphene nanocomposite, Clean Soil Air Water, 41 (2013) 992–1001.
[27] M. Ghorbani, A. Shams, O. Seyedin, N.A. Lahoori, Magnetic ethylene diamine-functionalized graphene oxide as novel sorbent for removal of lead and cadmium ions from wastewater samples, Environ. Sci. Pollut. Res. Int., 25 (2018) 5655–5667.
[28] F. Guo, Y. Liu, H. Wang, G. Zeng, X. Hu, B. Zheng, T. Li, X. Tan, S. Wang, M. Zhang, Adsorption behavior of Cr(VI) from aqueous solution onto magnetic graphene oxide functionalized with 1,2-diaminocyclohexanetetraacetic acid, RSC Adv., 5 (2015) 45384.
[29] A.K. Geim, Graphene: status and prospects. Science, 324 (2009) 1530–1534.
[30] N.A. El Essawy, A. H. Konsowa, M. Elnouby, H.A. Farag, A novel one-step synthesis for carbon-based nanomaterials from polyethylene terephthalate (PET) bottles waste, J. Air Waste Manage. Assoc., 67 (2016) 358–370.
[31] N.A. El Essawy, S.M. Ali, H.A. Farag, A.H. Konsowa, M. Elnouby, H.A. Hamad, Green synthesis of graphene from recycled PET bottle wastes for use in the adsorption of dyes in aqueous solution, Ecotoxicol. Environ. Saf., 145 (2017) 57–68.
[32] H. Naeimi, M. Golestanzadeh, Highly sulfonated graphene and graphene oxide nanosheets as heterogeneous nanocatalysts in green synthesis of bisphenolic antioxidants under solvent free conditions, RSC Adv., 4 (2014) 56475–56488.
[33] Y. Ma, P. Jin, W. Lei, P. La, X. Du, D. Zhang, One-pot method fabrication of superparamagnetic sulfonated polystyrene/$Fe_3O_4$/graphene oxide micro-nano composites, J. Porous Mater., https://doi.org/10.1007/s10934-018-0557-8.

[34] P.N. Diagboya, B.I Olu-Owolabi, D. Zhou, B. Han, Graphene oxide–tripolyphosphate hybrid used as a potent sorbent for cationic dyes, Carbon, 79 (2014) 174–182.
[35] H. Naeem, M. Ajmal, S. Muntha, J. Ambreen, M. Siddiq, Synthesis and characterization of graphene oxide sheets integrated with gold nanoparticles and their applications to adsorptive removal and catalytic reduction of water contaminants, RSC Adv., 8 (2018) 3599–3610.
[36] J., Deng, Y. Liu, S. Liu, G. Zeng, X. Tan, B. Huang, X. Tang, S. Wang, Q. Hua, Z. Yan, Competitive adsorption of Pb(II), Cd(II) and Cu(II) onto chitosan-pyromellitic dianhydride modified biochar, J. Colloid Interface Sci., 506 (2017) 355–364.
[37] G. Box, D.W. Behnken, Some new three level designs for the study of quantitative variables, Technometrics, 2 (1960) 455–475.
[38] E. Pajootan, M. Arami, M. Rahimdokht, Application of carbon nanotubes coated electrodes and immobilized $TiO_2$ for dye degradation in a continuous photocatalytic electro-Fenton process, Ind. Eng. Chem. Res., 53 (2014) 16261–16269.
[39] N. Oger, Y.F. Lin, C. Labrugere, E.L. Grognec, F. Rataboul, F. Felpin, Practical and scalable synthesis of sulfonated graphene, Carbon, 96 (2016) 342–350.
[40] Z. Yang, R. Huang, W. Qi, L. Tong, R. Su, Z. He, Hydrolysis of cellulose by sulfonated magnetic reduced graphene oxide, Chem. Eng. J., 280 (2015) 90–98.
[41] H. Beydaghi, M. Javanbakht, A. Bagheri, P. Salarizadeh, H. Ghafarian-Zahmatkesh, S. Kashefic, E. Kowsaria, Novel nanocomposite membranes based on blended sulfonated poly(ether ether ketone)/poly(vinyl alcohol) containing sulfonated graphene oxide/$Fe_3O_4$ nanosheets for DMFC applications, RSC Adv., 5 (2015) 74054–74064.
[42] H. Wang, X. Yuan, Y. Wuc, X. Chen, L. Leng, H. Wanga, H. Li, G. Zeng, Facile synthesis of polypyrrole decorated reduced graphene oxide–$Fe_3O_4$ magnetic composites and its application for the Cr(VI) removal, Chem. Eng. J., 262 (2015) 597–606.
[43] K.S.W. Sing, D.H. Everett, R.A.W. Haul, L. Moscou, R.A. Pierotti, J. Rouquerol, T. Siemieniewska, Reporting physisorption data for gas/solid systems with special reference to the determination of surface area and porosity, Pure Appl. Chem., 57 (1985) 603–619.
[44] T.M. Petrova, L. Fachikov, J. Hristov, The magnetite as adsorbent for some hazardous species from aqueous solutions: a review, Int. Rev. Chem. Eng., 3 (2011) 134–152.
[45] S. Wan, J. Wu, S. Zhou, R. Wang, B. Gao, F. He, Enhanced lead and cadmium removal using biochar-supported hydrated manganese oxide (HMO) nanoparticles: behavior and mechanism, Sci. Total Environ., 616–617 (2018) 1298–1306.
[46] X. Guo, B. Du, Q. Wei, J. Yang, L. Hu, L. Yan, W. Xu, Synthesis of amino functionalized magnetic graphenes composite material and its application to remove Cr(VI), Pb(II), Hg(II), Cd(II) and Ni(II) from contaminated water, J. Hazard. Mater., 278 (2014) 211.
[47] S. Luo, X. Xu, G. Zhou, C. Liu, Y. Tang, Y. Liu, Amino siloxane oligomer-linked graphene oxide as an efficient adsorbent for removal of Pb(II) from wastewater, J. Hazard. Mater., 274 (2014) 145.
[48] Q. Huang, Y. Chen, H. Yu, L. Yan, J. Zhang, B. Wang, B. Du, L. Xing, Magnetic graphene oxide/MgAl-layered double hydroxide nanocomposite: onepot solvothermal synthesis, adsorption performance and mechanisms for $Pb^{2+}$, $Cd^{2+}$, and $Cu^{2+}$, Chem. Eng. J., 341 (2018) 1–9.
[49] M.-p. Wei, H. Chai, Y.-I. Cao, D.-z. Jia, Sulfonated graphene oxide as an adsorbent for removal of $Pb^{2+}$ and methylene blue, J. Colloid Interface Sci., 524 (2018) 297–305.
[50] S.C. Smith, D.F. Rodrigues, Carbon-based nanomaterials for removal of chemical and biological contaminants from water: a review of mechanisms and applications, Carbon, 91 (2015) 122–143.
[51] S. Wana, W. Ding, Y. Wang, J. Wu, Y. Gu, F. He, Manganese oxide nanoparticles impregnated graphene oxide aggregates for cadmium and copper remediation, Chem. Eng. J., 350 (2018) 1135–1143.
[52] Y. Li, J. He, K. Zhang, T. Liu, Y. Hu, X. Chen, C. Wang, X. Huang, L. Kong, J. Liu, Super rapid removal of copper, cadmium and lead ions from water by NTA-silica gel, RSC Adv., 9 (2019) 397–407.
[53] Z.-H. Huang, X. Zheng, W. Lv, M. Wang, Q.-H. Yang, F. Kang, Adsorption of lead(II) ions from aqueous solution on low-temperature exfoliated graphene nanosheets, Langmuir, 27 (2011) 7558–7562.
[54] J. Liu, H. Du, S. Yuan, W. He, Z. Liu, Synthesis of thiol-functionalized magnetic graphene as adsorbent for Cd(II) removal from aqueous systems, J. Environ. Chem. Eng., 3 (2015) 617–621.